Received: 27 September 2021 | Accepted: 12 July 2022

DOI: 10.1002/asna.20224008

Astronomische Nachrichten

ORIGINAL ARTICLE

Measurements of visual double stars with PISCO2 at the Nice 76-cm refractor in 2013–2014

René Gili[1†] | Jean-Louis Prieur[2,3] | Jean-Pierre Rivet[4] | Farrokh Vakili[4] | Marco Scardia[5,6] | Luigi Pansecchi[6] | Robert W. Argyle[7] | Josefina F. Ling[8] | Luca Piccotti[8,9] | Eric Aristidi[4] | Laurent Koechlin[2,3] | Daniel Bonneau[4] | Luca Maccarini[10] | Jocelyn Serot[11]

[1]Université Côte d'Azur, Observatoire de la Côte d'Azur, CNRS, Unité Mixte de Service Galilée, Nice, France

[2]Université de Toulouse – UPS-OMP – IRAP, Toulouse, France

[3]CNRS – IRAP, Toulouse, France

[4]Université Côte d'Azur, Observatoire de la Côte d'Azur, CNRS, Laboratoire Lagrange, Nice, France

[5]Université Côte d'Azur, Observatoire de la Côte d'Azur - C2PU, Nice, France

[6]INAF – Osservatorio Astronomico di Brera, Merate, Italy

[7]Institute of Astronomy, Cambridge, UK

[8]Departamento de Matemática Aplicada, Observatorio Astrónomico R.M. Aller, Universidad de Santiago de Compostela, Santiago, Spain

[9]Instituto Universitario de Investigación en Matemáticas y Aplicaciones, Universidad de Zaragoza, Zaragoza, Spain

[10]Desio, Monza and Brianza, Italy

[11]Institut Pascal – CNRS UMR 6602, Aubière, France

Correspondence
J.-L. Prieur, Université de Toulouse – UPS-OMP – IRAP, Toulouse, France.
Email: jean-louis.prieur@irap.omp.eu

Abstract

We present relative astrometric and photometric measurements of visual double stars made in 2013–2014 with PISCO2 installed at the 76-cm refractor of the Côte d'Azur Observatory in Nice (France). Our observation list contains orbital couples as well as double stars whose motion is still uncertain. Three different techniques were used for obtaining measurements: Lucky Imaging, Speckle Interferometry, and the Direct Vector Autocorrelation method. From our observations of 4,864 multiple stars, we obtained 4,952 new measurements with angular separations in the range 0″.1–14″ and an average accuracy of 0″.015. The mean error on the position angles is 1°.0. Most of the position angles were determined without the usual 180° ambiguity with the application of the direct vector autocorrelation technique and/or by inspection of the Lucky images or the long integration files. We managed to routinely monitor faint systems ($m_V \approx 9$–11) with large magnitude differences (up to $\Delta m_V \approx 5$). We have thus been able to measure 49 systems containing red dwarf stars that had been poorly monitored since their discovery, from which we estimated the stellar masses thanks to Gaia measurements. We also measured the magnitude difference of the two components of 318 double stars with an estimated error of 0.2 mag. Except for a few objects that have been discussed, our measurements are in good agreement with the ephemerides computed with published orbital elements, even for the double stars whose separation is smaller than the diffraction limit. Thanks to good seeing images and with the use of high-contrast numerical filters, we have also been able to obtain 455 measurements with an angular separation smaller than the diffraction limit of our instrumentation, and consistent with those obtained with larger telescopes. Finally, we report 378 measurements of the 296 new double stars that we found in the files obtained during the observations.

KEYWORD

stars: double stars: close, visual, binaries, red dwarfs – astrometry–photometry – techniques: speckle interferometry, Lucky imaging, direct vector autocorrelation – instruments: 76-cm refractor*

†Deceased in October 2018.

1 | INTRODUCTION

This paper presents the results of speckle observations of visual double stars made in 2013–2014 with the PISCO2 instrument (Pupil Interferometry Speckle camera and COronagraph, 2nd Version) installed at the 76-cm refractor telescope of the "Observatoire de la Côte d'Azur," (OCA) in Nice (France). In the previous paper (Gili et al. 2021), we reported the observations made in 2011–2012 with the first version of PISCO2. In this paper, we present observations made with PISCO2 in its fully operational version.

PISCO2 is a speckle camera that was specially designed for the 76-cm refractor telescope and was described in Gili et al. (2014). In 2013–2014, we continued our previous research program which aims at obtaining high angular resolution measurements of double stars with sensitive detectors by using the good image quality of the site and the optics of the large Nice refractor, which often provides diffraction-limited images. The final purpose is to contribute to a better knowledge of the apparent relative motion of long-period binaries so that very accurate orbits could be determined in the future and fundamental parameters such as stellar masses could be inferred from them. The work presented here is the continuation of the program described in Gili & Prieur (2012) and Gili et al. (2020, 2021) that will be referred to as Paper I, II, and III, hereafter.

We describe the list of our targets and the conditions of our observations in Section 2. We introduce our calibration and data-reduction procedures in Sections 3 to 4. We present and discuss our relative astrometric and photometric measurements in Section 5. Then in Section 6, we compare our measurements with the ephemerides computed with published orbital elements, when available. Finally, we discuss the few cases of the largest residuals and then focus on the measurements of double stars whose separation is smaller than the diffraction limit of our instrumentation.

2 | OBSERVATIONS

2.1 | Observing list

Our list of targets is the same as in our previous papers and was presented in Paper I. It basically includes all the visual double stars of the "Washington Double Star Catalog" (Mason et al. 2022; hereafter: WDS) for which new measurements are needed to improve their orbits and that are accessible with our instrumentation.

The calendar of the observations made in 2013–2014 is reported in Table 1, with the distribution of the observations during those years. We indicate the epoch in the first column and the corresponding number of observations in Col. 2. We then give the night distribution of those observations during the month in Col. 3, and the number of nights used for the observations in Col. 4. During that period, the main maintenance work concerned the optics; it consisted of dismounting the main lens and remounting it with new centering wedges in August 2013.

The distribution of the apparent magnitudes m_V of the double stars observed in 2013–2014 is presented in Figure 1a and the difference in magnitudes Δm_V between the two components is presented in Figure 1b. Those data were retrieved from the WDS catalog. The telescope aperture and detector sensitivity led to a limiting magnitude of $m_V \approx 14$ for the faintest companions, which corresponded to about $m_V \approx 12$ for the double star systems (see Figure 1a).

Using both the observational data from DR2 GAIA (ESA 2022), such as the $g_{\rm mag}$ photometric magnitude of the main component, the effective temperature $T_{\rm eff}$, the galactic interstellar absorption $A_{\rm mag}$ and the parallax $\pi_{\rm gaia}$ (in milli-arcseconds), we derived $G_{\rm mag}$, the absolute magnitude in the Gaia bandwidth:

$$G_{\rm mag} = g_{\rm mag} - A_{\rm mag} - 5. \times \log_{10}\left(1{,}000/\pi_{\rm gaia}\right) + 5.$$

And we were able to construct the color-magnitude diagram of those double systems, which is displayed in Figure 2. Out of the 641 objects whose parallax was measured by DR2 GAIA (ESA 2022), we plotted the 629 objects for which the relative uncertainty on the parallax was smaller than 50%.

This plot shows that our observations well sampled most of the main sequence down to the faint red M stars. Indeed, this is shown in Table 2, with the list of the 49 systems with red dwarf stars that have been observed in 2013–2014. This list was built from the spectral types found in the WDS catalog by selecting the K and M stars of luminosity class V of Table 3. However, it should be underlined that the spectral classification of close double stars is still poorly known.

In Table 2, we successively reported the WDS name in Col. 1, the discoverer's name of the double star system in Col. 2, the spectral type as given in the WDS, with the type of each component for some systems, in Col. 3, the visual magnitudes mV_1 and mV_2 of components 1 and 2 in Cols. 4 and 5, respectively, the $B–V$ color index as measured by Hipparcos in Col. 6, and the interstellar galactic absorption $A_{\rm absp}$ of those systems, from DR2 GAIA in Col. 7. The Hipparcos parallax $\pi_{\rm Hip}$ and its error $\sigma_{\pi_{\rm Hip}}$, the DR2 GAIA parallax $\pi_{\rm gaia}$ and its error $\sigma_{\pi_{\rm gaia}}$ are then given in Cols. 8, 9, 10, and 11, respectively. The effective temperature

TABLE 1 Calendar of the observations of double stars in 2013–2014

Month	Nobs.	Night distribution during the month	Nights
2013-01	89	= 22 + 60 + 1 + 6	4
2013-02	177	= 27 + 40 + 28 + 40 + 42	5
2013-03	192	= 42 + 43 + 20 + 49 + 10 + 28	6
2013-04	178	= 21 + 18 + 43 + 49 + 40 + 7	6
2013-05	84	= 22 + 4 + 27 + 15 + 16	5
2013-06	200	= 5 + 30 + 30 + 21 + 33 + 23 + 23 + 21	8
2013-07	323	= 30 + 19 + 34 + 38 + 20 + 20 + 43 + 45 + 31 + 43	10
2013-08	505	= 40 + 40 + 22 + 37 + 42 + 45 + 45 + 32 + 40 + 42 + 36 + 33 + 31 + 20	14
2013-09	263	= 28 + 32 + 47 + 20 + 20 + 31 + 52 + 33	8
2013-10	114	= 52 + 62	2
2013-11	87	= 2 + 65 + 20	3
2013-12	278	= 15 + 11 + 51 + 20 + 55 + 21 + 40 + 20 + 31 + 14	10
Total in 2013	2490		81
2014-01	153	= 15 + 65 + 21 + 31 + 21	5
2014-02	228	= 21 + 21 + 35 + 20 + 26 + 55 + 50	7
2014-03	259	= 57 + 7 + 40 + 50 + 50 + 55	6
2014-04	120	= 54 + 13 + 24 + 29	4
2014-05	292	= 42 + 43 + 20 + 49 + 30 + 28 + 80	7
2014-06	283	= 45 + 30 + 52 + 31 + 36 + 43 + 22 + 24	8
2014-07	226	= 42 + 43 + 25 + 49 + 38 + 29	6
2014-08	237	= 46 + 43 + 24 + 56 + 40 + 28	6
2014-09	0		0
2014-10	421	= 69 + 51 + 40 + 61 + 44 + 52 + 63 + 41	8
2014-11	142	= 36 + 55 + 30 + 21	4
2014-12	147	= 15 + 59 + 42 + 31	4
Total in 2014	2508		65

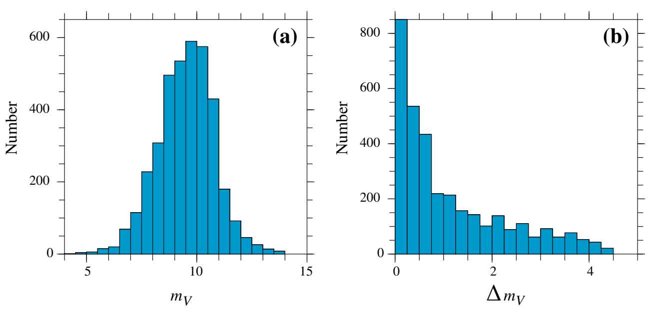

FIGURE 1 Distribution of the double star systems observed in 2013–2014: (a) Washington Double Star Catalog (WDS) visual magnitudes and (b) WDS magnitude differences Δm_V between the two components

$T_{\rm eff}$ from DR2 GAIA is displayed in Col. 12. The absolute magnitudes of components 1 and 2, MV_1 and MV_2, were then computed from mV_1 and mV_2, by using $A_{\rm absp}$ as the weighted average of the Hipparcos and GAIA parallaxes. They are given in Cols. 13 and 14, respectively. We finally give $\mathfrak{M}_2$ in Cols 15 and 16, respectively, which are some rough estimates of the masses of components 1 and 2, assuming that they follow the mass-luminosity relation.

We were able to construct the color-magnitude diagram of the double systems containing a red dwarf, using Table 2 by plotting MV_1 and MV_2 of Cols. 13 and 14 as a function of the color index B–V of Col. 6 (see Figure 3).

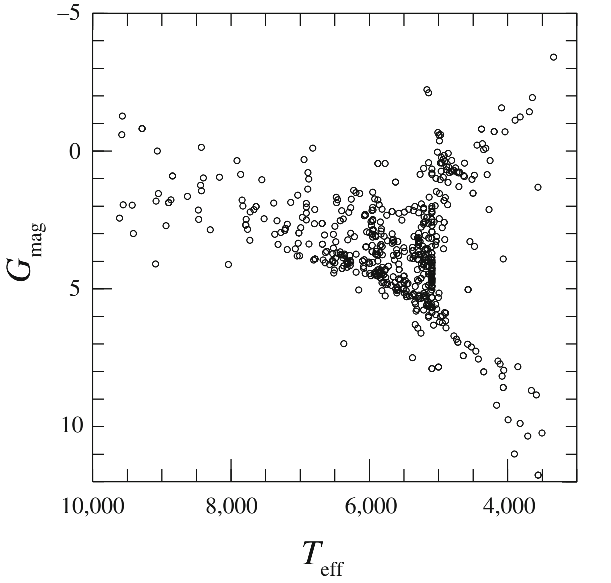

FIGURE 2 Color-magnitude diagram with the GAIA absolute magnitude G_{mag} versus the effective temperature T_{eff} of the double stars measured in Table 3, for which the GAIA parallaxes have a relative error smaller than 50% (i.e., 629 objects). This diagram was derived from the DR2 GAIA (ESA 2022) measurements

As proposed in Scardia et al. (2008) they used the mass-luminosity relation for class V stars:

$$\log_{10} \mathfrak{M} = -k\,(M_{bol} - M_0) \tag{1}$$

where $\mathfrak{M}$ is the mass of the star (in solar mass $M_\odot$), M_{bol} is its absolute bolometric magnitude, and k and M_0 are two constants. When fitting the relation (1) to Straizys & Kuriliene's (1981) data for the stellar class V (in the spectral range B0-M5), we obtained $k = 0.1{,}045$ and $M_0 = 4.60$ mag with a mean residual of 0.19 mag for the bolometric magnitudes. A more elaborated model of the mass-luminosity relation for stars of class V was proposed by Angelov (1993), with a 7th order polynomial instead of the first order polynomial of Equation 1, but our approximation is simpler and sufficient for our purpose, which is only qualitative.

We plotted in Figure 4 the individual masses that we computed for components 1 and 2 of those systems as a function of the parallax. The errors in our mass values are estimated at about 0.1 solar mass. They strongly depend on the errors of the parallaxes. The very small errors given by DR2 GAIA (ESA 2022) are unfortunately very optimistic.

Another problem concerns the spectral type of the components given by the WDS catalog. For many of those couples, the dynamical mass seems too large to leave some space for a red dwarf companion (Malkov 2012). This is also true for a triple system with a very small mass for the farthest companion, like WDS 22536 + 3756 = RUC 15, for which the third component has a minimum mass of M_3 such that $M_3 \sin i = 0.54\ M_\odot$ (see Pribulla 2006).

When examining the masses found in Cols 15 and 16, we found an inconsistency with the WDS spectral type reported in Col. 3 of Table 2 for some HDS1652 and BU 701 AB, which are only reported as K-type stars, whereas we found a mass larger than one solar mass for the components 1 of those two systems. We suggest a G + K spectral combination to account for those larger masses.

The subsample of systems containing red dwarfs that we reported in Table 2 should be considered as incomplete since precise spectral types and luminosity classes are still missing for many double stars in the WDS catalog.

2.2 | Optical setup and observing procedure

The observations reported here were made with PISCO2 mounted on the "Grand Equatorial" of the OCA Observatory. Since its free aperture diameter is $D = 74$ cm, the limit of diffraction is $\rho_D = \lambda/D = 0''.16$, at $\lambda = 570$ nm, corresponding to the average central wavelength of the filter we used.

When observing a single star, a two-aperture interferometer (with a D separation) placed on top of the telescope will generate a set of fringes angularly separated by λ/D in the image plane. When observing a double star made of two equal sources of light with a two-aperture interferometer, two sets of fringes will superimpose in the image plane. If the angular separation of the two stellar components is equal to half of the angular interfringe, the two sets of fringes cancel in the composite image. The smallest angular separation that can be measured for double stars with a two-aperture interferometer is then $\lambda/2D$, that is, $0''.008$ when $D = 7$ m (Michelson 1890), or $0''.08$ when $D = 70$ cm. This explains why we could resolve double stars closer than the diffraction limit of our instrument (see Section 6.3).

The PISCO2 instrument (Gili et al. 2014) was used with an ANDOR iXon DV897 EMCCD camera (ANDOR 2022) that was controlled by a dedicated acquisition and real-time processing program, `BuildSpeck1`, that was developed by J.-L. Prieur.

The instrumental setup and the observing procedure were the same as for the observations presented in Paper III. We invite the reader to look at this paper for more details.

All the files obtained during the observations were then examined and processed by R. Gili using various programs from the IRIS software (Buil 2022), the REDUC software (Losse 2022), and the program `Gdpisco`, developed by

TABLE 2 List of binary systems observed in 2013–2014 that contain a red dwarf star, with absolute magnitudes and masses of the two components that we derived from the Washington Double Star Catalog (WDS) and from GAIA measurements

WDS	Name	Spectral type	mV_1 (mag)	mV_2 (mag)	$B-V$ (mag)	A_{absp} (mag)	π_{Hip} (mas)	$\sigma_{\pi_{Hip}}$ (mas)	π_{gaia} (mas)	$\sigma_{\pi_{gaia}}$ (mas)	T_{eff} (°K)	MV_1 (mag)	MV_2 (mag)	$\mathfrak{M}_1$ ($M_\odot$)	$\mathfrak{M}_2$ ($M_\odot$)
00014 + 3937	HLD60	K0V + K1V	9.09	9.77	0.79	—	20.42	1.91	19.27	0.07	5190	5.52	6.20	0.76	0.63
00022 + 2705	BU733AB	G5Vb + K5V	5.83	8.9	0.70	0.11	80.63	3.03	79.07	0.56	5570	5.44	8.51	0.79	0.33
01076 + 2257	LDS9112AB	K4V + M3	8.42	14.67	1.12	0.38	48.20	1.06	48.69	0.07	4617	7.24	13.49	0.46	0.08
01267 + 1123	HDS188	M0V:	12.47	12.61	1.47	—	17.23	5.79	17.98	0.96	5000	8.73	8.87	0.28	0.27
04102 + 1722	HEI35	K2V + K6V	9.46	10.93	1.07	—	29.88	2.67	—	—	4796	6.84	8.31	0.53	0.34
04258 + 1800	COU2682	K2V	9.49	10.60	0.40	0.40	20.79	1.83	23.75	0.57	4950	6.70	7.81	0.55	0.42
05020 + 0959	HDS654	M3V:	11.84	12.83	1.54	—	31.20	8.56	41.92	0.08	4077	9.95	10.94	0.19	0.15
08286 + 3502	WOR19	M0V	11.51	11.55	1.57	—	51.13	6.64	—	—	—	10.05	10.09	0.20	0.20
08549 + 2612	A2131AB	G2V + K0V	6.95	9.02	0.67	—	21.70	1.32	23.01	1.11	5691	3.70	5.77	1.21	0.71
10084 + 1158	HDO127BC	K2V	8.24	13.2	0.89	0.13	42.09	0.79	41.21	0.08	5098	6.45	11.41	0.58	0.18
11035 + 5432	A1590	K2V	8.95	9.64	0.89	—	24.45	2.26	23.49	0.05	5190	5.81	6.50	0.68	0.57
11235 + 0701	BAG24Aa,Ab	M0V	10.37	10.37	1.57	0.72	—	—	31.23	0.81	4172	8.56	8.56	0.29	0.29
11374 + 4728	KU39	K4V	10.68	11.16	1.17	—	27.67	4.29	29.80	0.12	4514	8.05	8.53	0.38	0.34
11402 + 2609	HDS1652	K1V	8.40	11.24	0.93	—	—	—	7.45	0.36	4909	2.76	5.60	1.44	0.73
11520 + 4805	HU731	K0V	9.68	9.81	0.98	—	20.16	3.04	23.50	0.05	5143	6.53	6.66	0.59	0.57
11544 + 1515	WOR20	M0V	11.19	11.40	1.18	—	24.13	5.32	19.84	0.10	4964	7.69	7.90	0.36	0.34
12032 + 4751	VYS12AB	K4V	10.0	15.8	0.96	—	23.18	1.75	23.21	0.04	4700	6.83	12.63	0.51	0.13
12101 + 0526	WOR22AB	M0V	12.25	12.67	1.58	—	24.11	5.50	22.88	0.09	4472	9.05	9.47	0.26	0.23
12125 + 3940	HDS1727	M2V	11.72	13.14	1.46	1.90	34.10	7.62	31.80	0.33	3713	11.14	12.56	0.15	0.11
12422 + 2622	A1851	K4V	10.08	10.09	1.07	—	24.34	2.48	—	—	—	7.01	7.02	0.49	0.49
13048 + 5555	WOR23	M0V	11.24	12.21	1.58	—	31.44	3.62	28.96	0.04	4000	8.55	9.52	0.29	0.23
13063 + 2044	HU739	K4V	9.72	12.11	1.29	0.87	53.78	2.38	50.90	0.04	4122	9.13	11.52	0.29	0.16
13320 + 3108	WOR24	M0V	11.14	11.37	1.60	—	32.05	2.96	—	—	3906	8.67	8.90	0.28	0.27
13331 + 4316	COU1754	K8V	10.18	10.21	1.08	0.54	30.52	1.93	32.00	0.10	4634	8.24	8.27	0.33	0.33
13491 + 2659	STF1785	K4V + K6V	7.36	8.15	1.11	—	73.25	1.33	73.92	0.07	4707	6.70	7.49	0.53	0.42
13514 + 2620	YSC50Aa,Ab	K6V	11.7	12.1	1.37	—	20.99	2.33	—	—	—	8.31	8.71	0.34	0.31

TABLE 2 (Continued)

WDS	Name	Spectral type	mV_1 (mag)	mV_2 (mag)	$B-V$ (mag)	A_{absp} (mag)	π_{Hip} (mas)	$\sigma_{\pi_{Hip}}$ (mas)	π_{gaia} (mas)	$\sigma_{\pi_{gaia}}$ (mas)	T_{eff} (°K)	MV_1 (mag)	MV_2 (mag)	$\mathfrak{M}_1$ ($M_\odot$)	$\mathfrak{M}_2$ ($M_\odot$)
13514 + 2620	SKF260AB	K6V	11.0	13.5	1.37	—	20.99	2.33	—	—	—	7.61	10.11	0.41	0.22
14019 + 1530	ALD112	M2V	11.39	11.52	1.42	—	37.28	5.79	34.37	0.07	3854	9.07	9.20	0.24	0.24
14080 + 4535	FOX70	K8V	11.11	11.77	1.57	—	17.19	4.16	17.95	0.03	4417	7.38	8.04	0.41	0.35
14127 + 2349	YSC53	K0V	8.3	12.4	0.96	0.26	30.62	1.16	31.83	0.04	4976	6.07	10.17	0.66	0.25
14540 + 2335	REU2	M3V	12.24	12.66	0.90	—	97.83	5.99	87.94	0.18	3692	11.97	12.39	0.12	0.11
14562 + 1745	GII61AC	K5V	11.8	15.	1.34	—	11.64	3.68	16.31	0.29	4080	7.82	11.02	0.39	0.18
15038 + 4739	STF1909	F7V + K4V	5.20	6.10	0.65	—	78.39	1.03	77.24	1.20	5247	4.66	5.56	0.84	0.69
15360 + 3948	STT298AB	K2V	7.16	8.44	0.95	—	45.85	0.79	43.99	0.21	5095	5.40	6.68	0.75	0.55
17141–0824	BAR7	K3V	8.64	11.69	0.93	0.15	34.27	2.01	33.80	0.07	4916	6.44	9.49	0.57	0.27
17193–0221	RST4569AB	K3V	10.12	11.13	0.97	0.77	11.48	2.79	12.16	0.27	4893	6.30	7.31	0.59	0.46
17372 + 2754	KUI83AB	M0V:	9.81	10.40	1.16	—	32.05	2.28	—	—	—	7.34	7.93	0.39	0.34
18500 + 1519	YSC12AB	F8 + M2V	7.6	11.3	0.62	0.75	18.34	0.89	17.35	0.27	5841	4.58	8.28	0.86	0.30
19233–0635	HDS2745	K5V	9.85	13.19	1.09	0.25	31.38	2.27	32.10	0.04	4497	7.63	10.97	0.41	0.18
20302 + 2651	WOR9AB	M1V	10.50	10.63	1.34	—	43.24	4.37	49.03	0.91	4460	8.91	9.04	0.26	0.25
20396 + 0458	KUI99AB	K5V	8.28	9.63	1.24	—	53.82	2.21	—	—	4328	6.93	8.28	0.49	0.35
20501 + 2923	BAG28	K4V	8.32	12.4	1.07	—	48.38	1.77	49.43	0.05	4844	6.79	10.87	0.51	0.19
21000 + 4004	KUI103	M2V + M0.5V	10.49	12.40	1.51	—	66.21	2.54	66.81	0.09	3626	9.61	11.52	0.22	0.14
21379 + 2743	SKF245AC	M1V	9.9	15.0	1.50	0.11	76.07	2.53	76.22	0.04	4057	9.42	14.52	0.23	0.07
22234 + 3228	WOR11	M3.0V	11.59	12.01	1.57	—	62.18	10.01	65.86	0.10	3820	10.68	11.10	0.16	0.15
22281 + 1215	BU701AB	K0V	7.34	9.62	0.89	—	15.87	1.8	14.59	0.16	4955	3.18	5.46	1.33	0.77
22536 + 3756	RUC15	G5V + K9V	6.81	9.4	0.73	—	12.30	1.26	14.13	0.05	5248	2.55	5.14	1.58	0.69
23167 + 3441	HDS3315	K8V	11.25	11.75	1.57	0.78	10.53	1.89	11.80	0.22	4915	7.36	7.86	0.41	0.37
23405 + 2959	HDS3363	K4V	11.12	13.94	1.07	0.75	16.96	3.02	13.35	0.25	4485	7.54	10.36	0.43	0.22

TABLE 3 Table of binary measurements obtained with PISCO2 in 2013–2014 and *O–C* residuals with published orbits (Only the beginning in the printed version: the full table is available in the electronic version)

WDS	Name	Epoch	Bin.	ρ ($''$)	σ_ρ ($''$)	θ (°)	σ_θ (°)	Δm	Notes	Orbit	$\Delta\rho_{(O-C)}$ ($''$)	$\Delta\theta_{(O-C)}$ (°)
00002 + 3613	TDS1236	2013.944	1	0.480	0.009	152.8*	0.7					
00002 + 3613	TDS1236	2014.877	1	0.467	0.009	151.8	0.8					
00004 + 2749	TDS1238	2013.963	1	0.834	0.007	266.2*	0.8					
00005 + 2031	COU444	2013.924	1	0.693	0.007	39.5	0.3	3.25				
00010 + 2721	DAM361Aa,Ab	2013.927	1	1.442	0.007	358.3	0.3	2.26				
00010 + 2721	DAM361	2013.927	1	5.372	0.571	218.8	5.5					
00011 + 2502	POU5882	2013.927	1	1.302	0.007	42.8	0.3	0.39				
00014 + 3937	HLD60	2013.867	1	1.309	0.013	168.5*	0.3			Izm2019	−0.00	0.9
00014 + 3937	HLD60	2014.828	1	1.322	0.015	167.5*	0.3			Izm2019	0.01	0.3
00014 + 4828	COU1850AB	2014.831	1	0.684	0.020	7.9*	0.8					
00014 + 4828	COU1850Aa,Ab	2014.831	1	0.126	0.052	111.9	4.9					
00022 + 2705	BU733AB	2013.818	1	0.520	0.011	313.8*	0.3			Sod1999	0.01	−5.0
00022 + 2705	BU733AB	2013.818	1	0.527	0.007	312.1*	0.4			Sod1999	0.01	−6.7
00022 + 2705	BU733AB	2014.869	1	0.432	0.038	352.0	5.3			Sod1999	0.06	1.3
00022 + 2705	BU733AB	2014.869	1	0.424	0.009	349.7	1.8			Sod1999	0.05	−1.0
00022 + 2705	BU733AB	2014.877	1	0.449	0.024	347.2	2.8			Sod1999	0.08	−3.8
00022 + 2705	BU733AB	2014.877	1	0.462	0.030	357.6	7.6			Sod1999	0.09	6.6

Note: In column 7, the * indicates that the position angle θ could be determined without the 180° ambiguity. In column 13, the superscript *Q* indicates that our θ measurement quadrant was not compatible with the quadrant used for computing the orbit. The full table is available as part of the supporting online material.

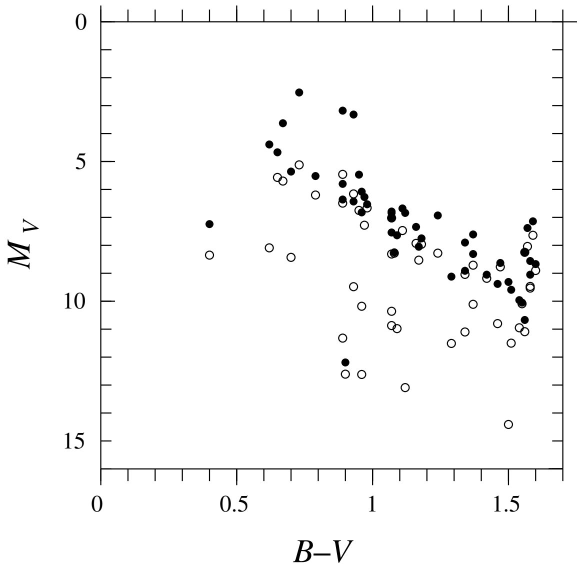

FIGURE 3 Color-magnitude diagram with the absolute visual magnitude M_V versus the B–V index of the double stars measured in Table 3 that contain a red dwarf component. The locations of the primary and secondary components are drawn as filled and open circles, respectively

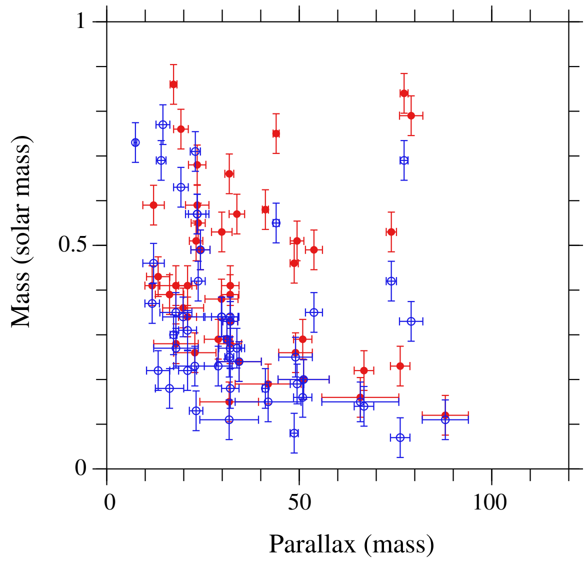

FIGURE 4 Mass versus parallax diagram of the double stars measured in Table 3 that contain a red dwarf component. The masses M_1 and M_2 of components 1 and 2 are drawn as red and blue circles, respectively

J.-L. Prieur. In that program, some high-contrast numerical filters were implemented in 2013–2014 thanks to R. Gili's suggestions. Those files were re-processed in 2021 and 2022 by J.-L. Prieur in order to obtain another independent confirmation of those results. A systematic search was also done in the WDS catalog, and all our measurements were compared with other values obtained by observers in this catalog. We have found a very good agreement for the position angle measurements in general, but we found some discrepant values for the angular separation, with a factor of two as the difference. This may be due to the bad binning value that was noted during the observations. We have corrected them when we found them, but some other cases may exist that we have not yet found. Unfortunately, R. Gili is deceased and cannot give us explanations for this problem any longer.

3 | SCALE AND POSITION ANGLE CALIBRATIONS

The astrometric calibration of the magnification scale of PISCO2 was done with a calibration grating mask (see Paper II). The scale value was found to be $0''.0738$/pixel when the frames were not binned (xbin = 1, ybin = 1). In that case, the diffraction limit in V of $0''.16$ (see Section 2.2) corresponds to 2.16 pixels, which is in agreement with Shannon's sampling criteria (i.e., the diffraction diameter is sampled by more than two pixels).

The calibration of the origin of the position angles was done by recording star trails caused by the diurnal motion. The orientation of our images on the detector was approximately conventional, with North at the bottom, and East at the right. After measuring a series of star trail images, we found: $\theta_{\rm sky} = 90.99 + \theta_{\rm frame}$, where $\theta_{\rm sky}$ and $\theta_{\rm frame}$ are the angular positions on the sky and on the EMCCD frame in degrees, respectively.

4 | DATA REDUCTION PROCEDURE

Most of the high angular resolution observations presented here have been obtained with the "speckle interferometry" technique that was derived from the pioneering work of Labeyrie (1970). More precisely, we have used the method described in Worden et al. (1977) which works with a "flattened" autocorrelation and is routinely used for PISCO (see Scardia et al. 2019, for instance). The whole processing was done in two steps: real-time processing with the `BuildSpeck1` program and post-processing with programs like `Gdpisco` (see Paper III for more details).

The 180°-ambiguity of speckle measurements related to the position angles of double stars was mostly solved by the direct vector autocorrelation (DVA) method, as proposed by Bagnuolo et al. (1992), which computes the "oriented" autocorrelation function and takes into account the brightness level of the vector ends. The DVA both allows the quadrant determination and the measurement of Δm when the contrast is not too large (e.g., $\Delta m < 2$).

In the case of good seeing conditions, we obtained high-resolution images with the Lucky Imaging method implemented in the REDUC software (Losse 2022). This method was described in Paper I and consists of shift-and-add processing of a subset of selected good images. We could measure couples with very large differences of brightness, up to 3–4 magnitudes (see Section 5). Compared to speckle interferometry, the main advantage of "Lucky imaging" is to provide a full image which is convenient for the determination of the quadrants (where the companion stands) and of the difference in magnitudes between the two components.

5 | RELATIVE ASTROMETRIC AND PHOTOMETRIC MEASUREMENTS

The relative astrometric and photometric measurements that we obtained with PISCO2 in 2013–2014 are displayed in Table 3 (in the printed version of this paper, only the beginning of this table is printed; the full version is only available in electronic form). They concern 4,864 visual double stars or multiple objects, with 4,952 position measurements and 567 cases of unresolved observations.

In this table, for each object, we successively give its WDS name in Col. 1, the official double star designation in Col. 2 (sequence is "discoverer-number," with its components if that is the case), the epoch of observation in Besselian years (Col. 3), the binning factor used by the detector when acquiring the image (Col. 4), the angular separation ρ (Col. 5) between the two components with its error (Col. 6) in arcseconds, and the position angle θ (Col. 7) with its error (Col. 8) in degrees, measured from the North and positive to the East, the measured difference of magnitudes Δm between the two components (Col. 9), and some notes in Col. 10 ("NDg" or "ND" for new doubles, and "NR" for "Not Resolved").

The $(O - C)$ (Observed minus Computed) residuals of the measurements for the systems with a known orbit are displayed in Cols. 12 and 13 for the residuals in angular separation and position angle, respectively. The orbital elements used for computing the ephemerides were retrieved from the "Sixth Catalogue of Orbits of Visual Binary Stars" (Hartkopf et al. 2001; Matson et al. 2022, hereafter OC6). The corresponding authors are given in Col. 11, using the style of the OC6 references.

The difference of magnitudes Δm with the wide-band filter that we used for the observations (see Paper I), was obtained either from the Lucky Imaging or the DVA method, is reported in Col. 9, and concerns 318 objects (see Figure 5b). By comparing the measurements obtained for the same objects, we estimated the average (internal) errors at about 0.2 mag.

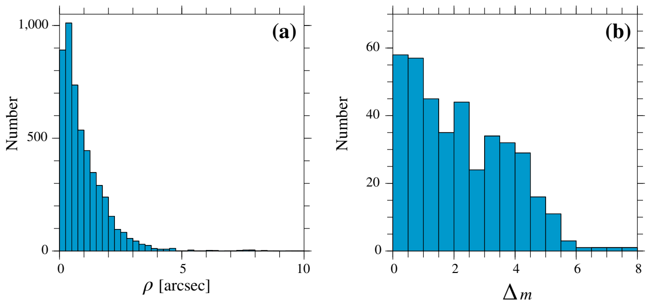

FIGURE 5 Distribution of the double star systems observed in 2013–2014: (a) angular separations of the measurements (with a limited range in angular separation for better visibility, since there are very few large separations), and (b) differences of magnitude Δm measured with Lucky Imaging and direct vector methods

The distribution of the 4,952 angular separations measured in this paper is displayed in Figure 5a and shows a maximum of $\rho \approx 0''.4$. The largest separation of $\rho = 14''.5$ was obtained for HJ477AC. The smallest separation was measured for COU773 with $\rho = 0''.08$. This is smaller than the diffraction limit $\rho_D = \lambda/D = 0''.16$, with our V filter (i.e., $\lambda = 570$ nm) and our refractor, whose free aperture is $D = 0.74$ m. The residuals of our measurements with published orbits will be discussed in Section 6.

A * was added to the θ measurements in Col. 7 when we could determine the quadrants of the measurements, that is, when our observations allowed us to solve the 180° ambiguity of the autocorrelation frames. When this was not possible, we used the quadrant of the last observations from the WDS catalog. Eventually, when such observations were missing, we assumed that the quadrant was equal to 1 or 2 (i.e., the companion was lying in the [0°, 90°] or [90°, 180°] sectors).

A superscript Q was added to the θ residuals in Col. 13 when the quadrants of our measurements were not in agreement with those used for the orbits.

The average errors determined by our `Gdpisco` program are $0''.015 \pm 0''.122$ and $1°.0 \pm 1°.8$ for ρ and θ respectively. Those errors were computed for each measurement by estimating the uncertainties in the background estimation and are consistent with the variations seen in repeat measurements of the same systems. Indeed, the background removal of the autocorrelation spots is the critical step of the measurement procedure. Since the frame scale was $0''.0738$/pixel, those values indicate that the location of the secondary peaks of the autocorrelations was determined with a mean accuracy of about 1/5th of a pixel.

During his observations, R. Gili found some new stellar components around double stars that were previously known. This concerns 121 measurements of 81 new double stars that we discovered in 2013–2014, and it is indicated by "NDg" in Col. 10 of Table 3. A subset of those

TABLE 4 Table of measurements of the new double stars discovered by R. Gili during his observations: (121) new measurements of the 81 “NDg” objects of Table 3

WDS	Name	Epoch	Bin.	ρ ($''$)	σ_ρ ($''$)	θ (°)	σ_θ (°)	Δm	Notes
00026 + 1841	HDS2AC	2013.818	1	2.045	0.010	156.7*	0.3		
00037 + 1851	XMI104BC	2013.924	1	0.982	0.007	176.5	0.3	3.43	
00084 + 1843	COU246Aa,Ab	2014.973	1	0.248	0.007	195.0	1.1		
00115 + 3556	HDS24Aa,Ab	2013.946	1	0.102	0.017	121.7	4.9		
00124 + 4558	HDS27AC	2014.976	1	1.390	0.015	126.3	0.5		
00175 + 2200	COU73Aa,Ab	2013.944	1	0.106	0.050	48.0	7.3		
00310 + 2839	CTU1AC	2013.944	1	1.338	0.007	53.3*	0.3		
00495 + 4018	HDS110Aa,Ab	2014.976	1	0.108	0.042	126.4	7.1		
00495 + 4018	HDS110Aa,Ab	2014.976	1	0.128	0.042	130.1	7.1		
01042 + 2256	GIC19Aa,Ab	2013.927	1	1.205	0.007	266.1	0.3	0.29	
01076 + 2257	LDS9112Aa,Ab	2013.927	1	1.474	0.007	72.9	0.3	4.38	
01291 + 1040	XMI205BC	2013.966	1	0.921	0.007	213.7	0.3	6.27	
02270 + 1952	A2328AC	2013.835	1	1.247	0.007	95.4	0.3		
02270 + 1952	A2328AC	2013.836	1	1.244	0.007	95.6	0.3	3.31	
02480 + 1604	TDS96Aa,Ab	2014.059	1	0.187	0.011	186.1	3.6		
04112 + 5555	HDS531AC	2014.973	1	1.787	0.010	75.3	0.3		
04112 + 5555	HDS531AD	2014.973	1	3.068	0.017	80.7	0.3	1.43	
04362 + 0814	A1840AC	2013.111	1	3.250	0.028	114.2	0.8		
05116 + 1132	HEI459AC	2014.149	1	3.190	0.027	279.9*	9.7		GII76AC
05116 + 1132	HEI459AC	2014.149	1	3.105	0.018	280.4	0.3		
05287 + 2317	COU84AC	2013.130	1	4.579	0.070	111.4	0.3		
05287 + 2317	COU84AC	2013.130	1	4.632	0.023	111.4	0.3		
05287 + 2317	COU84AC	2013.136	1	4.607	0.023	111.4*	0.3	4.33	
05512 + 2235	COU373AC	2014.059	1	2.531	0.036	189.3*	0.5		
05529 + 2800	COU899Aa,Ab	2013.111	1	0.215	0.027	155.0*	2.3		
05529 + 2800	COU899Aa,Ab	2014.059	1	0.229	0.017	160.7	2.3	0.10	
05563 + 2005	COU375AC	2013.106	1	4.147	0.021	41.1*	0.3	2.96	
05563 + 2005	COU375AD	2013.108	2	8.360	0.042	140.9*	0.3	1.63	
06347 + 2605	J1093AC	2014.182	1	1.839	0.011	267.6	0.5		
06347 + 2605	J1093AC	2014.857	1	1.841	0.013	267.6*	0.3		
06564 + 1029	HEI712AC	2014.149	1	3.148	0.025	339.5*	1.3		
07032 + 3457	GII82Aa,Ab	2014.201	1	0.328	0.007	174.6	0.3	0.35	Close to COU1739
07032 + 3457	GII82Aa,Ab	2014.201	1	0.303	0.024	176.0	2.0		
07032 + 3457	GII82Aa,Ab	2014.206	1	0.327	0.007	174.7	0.3	0.46	
07271 + 2718	COU1108AC	2013.158	1	3.575	0.037	14.1	1.7		
08002 + 1557	GII81AC	2014.206	1	0.217	0.007	33.9	0.3	0.57	Close to A2885
08452 + 1941	BOV54AC	2013.158	1	5.277	0.026	287.0	0.3	1.75	
08536 + 1210	GII38Ba,Bb	2013.205	1	0.234	0.007	348.6	0.3	0.03	HEI480

TABLE 4 (Continued)

WDS	Name	Epoch	Bin.	ρ ($''$)	σ_ρ ($''$)	θ ($^\circ$)	σ_θ ($^\circ$)	Δm	Notes
08536 + 1210	GII38AC	2013.205	1	1.520	0.008	271.0	0.3	4.15	HEI480
09007 + 3208	COU1253AC	2014.513	1	1.714	0.021	47.9	0.4		
09062 + 3314	GII37Ba,Bb	2013.158	1	0.286	0.007	264.3*	0.3		Close to COU1560
09062 + 3314	GII37Ba,Bb	2014.201	1	0.344	0.007	266.6	0.3	0.10	
09509 + 2016	GII80Ba,Bb	2014.198	1	0.235	0.007	234.7	0.3	0.09	Close to COU49
09509 + 2016	GII80Ba,Bb	2014.206	1	0.208	0.007	238.8	0.3	0.11	
Close to COU49 10353 + 7140	GII59AC	2013.298	2	6.955	0.035	153.9	0.3	0.58	
11062 + 1018	GII58AC	2013.287	1	1.835	0.009	343.9	0.3	4.26	
11062 + 1018	GII58AC	2013.287	1	1.815	0.013	343.7*	0.4		
11062 + 1018	GII58AC	2013.295	1	1.867	0.010	343.3	0.3		
11062 + 1018	GII58AC	2013.297	1	1.811	0.009	344.3	0.3	4.41	
11062 + 1018	GII58AC	2014.273	1	1.765	0.023	343.3*	0.3		Close to TDS7663
11322 + 3615	HU1134AC	2014.240	1	2.951	0.015	277.8*	0.3		
11323 + 2527	GII83AC	2014.248	1	1.027	0.007	173.1*	0.3		
11323 + 2527	GII83AC	2014.250	1	1.072	0.007	172.2*	0.7		Close to TDS7612
11372 + 0450	HEI852AC	2013.585	1	0.897	0.013	65.9	0.8		
11539 + 2020	HU1256AC	2013.347	1	1.433	0.016	348.1*	0.7		
11539 + 2020	HU1256AC	2013.347	1	1.433	0.025	347.4	0.7		
13064 + 2217	WSI104AC	2013.645	1	0.460	0.007	38.0	0.3		
13276 + 2116	GII60AC	2013.339	1	2.855	0.023	127.4*	0.3		
13276 + 2116	GII60AC	2014.333	1	2.920	0.015	127.9	0.3		
13276 + 2116	GII60AC	2014.333	1	2.895	0.014	128.0	0.3		
14113 + 3013	COU605AC	2013.451	2	2.025	0.046	126.1	0.5		
14178 + 4845	HJ2710AB	2014.428	1	1.160	0.027	7.6	2.3		
14178 + 4845	HJ2710AB	2014.428	1	1.160	0.011	8.5	1.0		
14269 + 5602	HDS2037AC	2014.404	1	1.807	0.017	14.0	0.4		
14562 + 1745	GII61AC	2013.429	1	1.824	0.010	195.0*	0.3		Close to HDS2108
14562 + 1745	GII61AC	2013.432	1	1.851	0.009	196.6*	0.5		
14562 + 1745	GII61AC	2013.451	1	1.741	0.009	195.9	0.3	4.23	
14562 + 1745	GII61AC	2013.454	1	1.717	0.009	196.6*	0.5		

Table of measurements of new double stars discovered by R. Gili in 2013–2014

WDS	Name	Epoch	Bin.	ρ ($''$)	σ_ρ ($''$)	θ ($^\circ$)	σ_θ ($^\circ$)	Δm	Notes
14562 + 1745	GII61AC	2013.456	1	1.704	0.009	194.2	0.3	4.02	
14562 + 1745	GII61AC	2014.404	1	1.793	0.009	194.9*	0.3		
15371 + 2646	GII40AC	2013.432	1	2.100	0.011	240.8*	0.3		Close to HDS2199
15371 + 2646	GII40AC	2013.451	2	2.126	0.022	242.7	0.3		
15371 + 2646	GII40AC	2013.454	1	2.136	0.013	241.5	0.3		
15371 + 2646	GII40AC	2014.412	1	2.089	0.010	242.9	0.3		
15371 + 2646	GII40AC	2014.420	1	2.080	0.010	242.9	0.7		

TABLE 4 (Continued)

WDS	Name	Epoch	Bin.	ρ ($''$)	σ_ρ ($''$)	θ (°)	σ_θ (°)	Δm	Notes
15484 + 3931	COU1446AC	2014.393	1	7.836	0.039	159.4*	0.3		
16192 + 2553	COU412Aa,Ab	2014.421	1	0.351	0.023	292.1*	1.7		
16199 + 3943	KUI72AC	2014.434	1	3.147	0.032	125.1	0.3		
16268 + 1203	A1859AC	2013.106	1	1.736	0.009	23.9	0.5		
16385 + 3006	TDT16AC	2013.498	1	0.967	0.014	72.1	1.0		
17168 + 0133	TDT296AC	2013.566	1	3.652	0.021	19.4*	0.3		
17284–0201	RST4571Aa,Ab	2013.588	1	0.243	0.007	62.9	5.6		
17284–0201	RST4571Aa,Ab	2013.612	1	0.258	0.007	60.2	6.3	1.25	
17284–0201	RST4571Aa,Ab	2013.614	2	0.235	0.007	68.3*	0.3		
17357 + 0409	A2985AC	2013.555	1	3.286	0.016	178.7	0.3		
17532 + 3243	GII43Aa,Ab	2013.555	1	0.223	0.018	9.9	1.8		Close to COU998
17532 + 3243	GII43Aa,Ab	2014.443	2	0.224	0.014	16.8*	1.2		
17539 + 1413	TDT563Aa,Ab	2013.585	1	0.522	0.010	107.0*	0.3		
17549 + 2713	TDT568AC	2013.645	1	1.813	0.012	90.2	0.4		
18349 + 0556	GII66AC	2013.626	1	3.097	0.015	133.0	0.3		Close to TDT945
18349 + 0556	GII66AC	2014.767	1	3.114	0.016	132.9	0.3	3.31	
18416–0522	GII65	2013.613	1	1.992	0.010	357.5*	0.3	1.92	Close to TDT1001
18427 + 0742	HEI870Aa,Ab	2013.580	1	0.907	0.007	246.1*	0.3		
18427 + 0742	HEI870Aa,Ab	2013.585	1	0.883	0.007	245.5*	0.3		
18486 + 3132	TDT1063AC	2013.640	1	1.089	0.012	141.7	1.8		
18597 + 2949	COU1019AC	2013.730	1	5.757	0.029	51.5	0.3		
19037 + 1133	GII63Aa,Ab	2013.610	1	0.472	0.007	137.5	0.9		Close to HEI567
19037 + 1133	GII63AC	2013.598	2	5.259	0.026	117.1	0.3	4.22	
19037 + 1133	GII63AC	2013.611	1	5.302	0.027	117.1	0.3	4.50	
19082 + 1215	MCA54AC	2013.566	1	1.138	0.028	101.2	1.7		
19345 + 0037	BAL1206Aa,Ab	2013.610	1	0.585	0.018	288.7*	1.9		
20014 + 1045	TOK34AC	2013.643	1	3.587	0.018	175.0	0.3	2.25	
20014 + 1045	TOK34AC	2013.643	1	3.565	0.018	175.4	0.3		
20168 + 3206	COU1476AC	2014.601	1	3.013	0.293	156.7	3.3		
20188 + 3507	A286AC	2014.620	1	4.414	0.022	59.4	0.3		
20227 + 2837	COU1169AC	2013.946	1	1.711	0.009	175.3	0.3		
20348 + 1726	COU223AC	2013.678	1	1.318	0.008	287.7*	0.3		
21451 + 3424	COU1186AC	2013.946	1	1.716	0.009	174.9	0.3		
21531 + 4826	GII87AC	2014.831	1	6.262	0.031	31.2	0.3	3.78	Close to COU2319
21585 + 2601	COU838AC	2013.542	1	1.649	0.008	122.2	0.7	0.04	
22454 + 5129	HU783AC	2014.814	1	4.033	0.020	103.9	0.3		
22569 + 3935	GII89Aa,Ab	2014.552	1	0.240	0.007	260.4	1.0		Close to COU1841
22595 + 4355	COU2146AC	2014.776	1	3.628	0.018	145.2	0.3		
22595 + 4355	COU2146AC	2014.776	1	3.632	0.018	325.1	0.3		

TABLE 4 (Continued)

WDS	Name	Epoch	Bin.	ρ ('')	σ_ρ ('')	θ (°)	σ_θ (°)	Δm	Notes
23022 + 1832	HDS3279AC	2014.814	1	0.691	0.022	121.9	2.3		
23022 + 1832	HDS3279AD	2014.814	1	1.657	0.025	163.1	2.3		
23022 + 1832	HDS3279AD	2014.814	1	1.662	0.008	163.4	0.4		
23033 + 1129	GII71Aa,Ab	2013.818	1	0.220	0.047	24.4	7.5		Close to ROE132
23033 + 1129	GII71Aa,Ab	2013.820	1	0.149	0.050	32.7	8.0	0.69	
23040 + 2414	TDT3870AC	2014.828	1	4.283	0.025	85.7*	0.3		
23504 + 3926	COU1200Aa,Ab	2013.946	1	0.177	0.007	83.0	1.1		

*indicates that θ was determined with our quadrant value (or with the long integration).

measurements is reported in Table 4. This table has the same column description as Table 3, which was described at the beginning of this section. Some of them have been monitored since their discovery and are included in the list of René Gili's new double-star discoveries (Gili 2016). In Table 4, they correspond to the objects whose names start with GII. More observations are required to confirm the other new couples at this table.

We also found 215 new components during the processing stage, mainly very close components that were not seen by R. Gili during the observations. In agreement with the current denomination adopted by the WDS, we noted the corresponding couples as "Aa, Ab" or "Ac" in Col. 2 of Table 3, with the mention "NDp" in Col. 10 of this table. Some of these have been observed many times, but most of them will have to be confirmed by new observations. We encourage other observers to confirm our discovery.

6 | RESIDUALS WITH PUBLISHED ORBITS

6.1 | Comparison with published ephemerides

The residuals from published orbits that have been computed with our measurements in Table 3 are plotted in Figure 7a. Among those 486 residuals, this plot gives the names of 10 objects with the largest residuals, which will be discussed in Section 6.2. The other residuals are well centered around the origin, with a rather large scatter.

The mean values computed with the residuals of Table 3 are $<\Delta\rho_{O-C}>= 0''.008 \pm 0''.053$ and $<\Delta\theta_{O-C}>= -0°.02 \pm 3°.5$ (after rejecting the outliers). In both cases, the offsets are very close to zero, with absolute values much smaller than the *SD*s, which provides validation of our calibration (see Section 2.2). The rather large *SD* can be explained by the poor quality of many orbits due to their old age and the lack of observations. Indeed, we have checked that our measurements are in good agreement with the observations reported in the "Fourth Catalogue of Interferometric Measurements of Binary Stars" (Hartkopf et al. 2020, Hartkopf et al. 2001 hereafter IC4) when they were present in this catalog.

The measurements with the largest residuals from Table 3, such that $\Delta\rho > 0''.1$ or $\Delta\theta_{O-C} > 10°$, are reported in Table 5. Some examples of autocorrelations of those double stars are shown in Figure 6. The content of this table has the same notation as Table 3. In the last column, we added the other measurements that are reported in the IC4 or the WDS catalog for similar epochs. These are in fair agreement with ours.

In Table 5, we see that our measurements are in fair agreement with the published orbits, as we will see in the next section. However, most of those objects have been poorly monitored until now, and their orbits still need additional measurements to be more precise.

If we consider the best orbits only, for instance, the orbits of Grade 1 in OC6, the plot of the residuals of Table 3 becomes much more concentrated (see Figure 7b). This shows that the dispersion in Figure 7a is caused by the poor quality of most of the orbits.

6.2 | Discussion on the objects with the largest residuals

We discuss here the cases of the measurements with the largest residuals that appear as outliers in Figure 7a, that is, A700, A1061AB, A2157, A2479, AG331, BU1235, COU206, COU1006, COU1212, and WOR23.

The case of A700 is particular and was already discussed in Paper III. The relative motion of the pair suggests that it is an optical double star rather than a physical binary. A rectilinear solution was computed by Parent et al. (2017).

TABLE 5 Measurements made in 2013–2014 with large residuals: values with $|\rho_{O-C}| > 0''.1$ or $|\theta_{O-C}| > 10°$

WDS	Name	Epoch	ρ ($''$)	σ_ρ ($''$)	θ (°)	σ_θ (°)	Orbit	$\Delta\rho_{(O-C)}$ ($''$)	$\Delta\theta_{(O-C)}$ (°)	Grade	Other measurements, ρ ($''$) θ (°)
00167 + 3629	STT4	2014.976	0.170	0.023	25.7	3.4	Alz2000a	0.01	−12.9	2	[IC4-2007: 0.23 99.7]
00583 + 2124	BU302	2014.976	0.320	0.018	220.4	2.9	Cve2006e	0.14	−19.3	4	[IC4-2008: 0.30 206.6]
01105 + 3917	COU1212	2013.944	0.269	0.017	174.3*	2.9	Cou1999b	−0.27	51.2^{Q}	5	[WDS-1995: 0.2 286]
01345 + 3440	A1913AB	2013.941	0.422	0.008	129.5*	0.3	Baz1987d	0.16	34.9^{Q}	4	[IC4-2009: 0.40 313.9]
01462 + 3343	HU804	2013.944	0.300	0.027	76.1*	3.6	Ole2001	−0.12	3.3	5	[IC4-2009: 0.28 68.8]
01570 + 3101	A819	2013.963	0.140	0.050	0.6*	8.0	Hrt2009	−0.10	12.6	3	[IC4-2007: 0.18 315.3]
03023 + 1820	A2414	2013.015	0.525	0.017	68.3*	2.3	Hei1997	0.17	−16.3	5	[IC4-2009: 0.524 67.8]
04216 + 0658	A1835	2013.013	0.207	0.019	9.3	1.5	Zir2010	−0.00	−13.5	4	[IC4-1996: 0.159 350.3]
04245 + 2244	BU1235	2013.016	0.125	0.050	327.2	8.0	Zir2010	0.06	59.0	4	[IC4-1996: 0.239 62.3]
04445 + 3953	COU1524	2014.119	0.098	0.050	62.7	8.0	Doc2019f	−0.03	23.1^{Q}	4	[IC4-2011: 0.146 62.3]
06105 + 2300	BU1058	2014.182	0.082	0.050	208.6*	8.0	FMR2014b	−0.07	-10.6^{Q}	4	[IC4-2011: 0.104 229.4]
06200 + 2826	BU895AB	2013.044	0.182	0.007	164.1	5.8	Hrt2000c	0.06	−23.5	2	[IC4-2008: 0.24 158.9]
06594 + 2514	A1061AB	2014.146	0.083	0.050	73.2	8.0	USN2002	−0.11	−73.1	5	[IC4-1999: 0.62 42.4]
07123 + 1839	AG331	2013.169	0.266	0.017	213.7*	1.4	Izm2019	0.17	69.2	5	[IC4-2000: 0.39 201.3]
08095 + 3213	STF1187AB	2014.248	3.077	0.015	21.2	0.3	Ole2001	0.13	0.7	5	[IC4-2004: 0.164 141.8]
08183 + 3859	STF1211AB	2014.248	0.317	0.027	178.1*	1.7	Hei1996c	−0.01	14.8	5	[IC4-2004: 0.218 272]
08423 + 2002	COU382	2013.158	0.331	0.017	356.1*	2.2	Cou1999b	0.21	16.1^{Q}	5	[IC4-2008: 0.244 177]
08423 + 2002	COU382	2014.198	0.325	0.017	356.8*	1.5	Cou1999b	0.21	19.9^{Q}	5	[IC4-2008: 0.244 177]
08539 + 1958	COU773	2014.198	0.079	0.050	74.2	8.0	Cou1999b	−0.10	13.6	4	[IC4-2007: 0.165 62.2]
08585 + 3548	COU1897	2013.196	0.142	0.015	305.7	2.9	Doc2013b	0.06	13.8	3	[IC4-2010: 0.09 267.5]
09376 + 1528	A2479	2014.198	0.412	0.007	191.4*	0.5	Hei1978a	0.14	−56.0	5	[IC4-2008: 0.392 183.4]
09477 + 2036	COU284	2013.287	0.139	0.024	340.1	1.8	Doc2019c	0.06	-25.0^{Q}	4	[IC4-1997: 0.120 46.2]
10121 + 2118	A2146	2013.287	0.113	0.050	179.9	8.0	Hei2001	−0.08	−30.3	4	[IC4-2008: 0.237 162.1]
11162 + 3136	A2157	2013.221	1.335	0.009	2.5*	0.3	Pop1996b	0.27	-54.3^{Q}	5	[IC4-2008: 1.363 1.1]
11162 + 3136	A2157	2014.333	1.344	0.009	2.4*	0.3	Pop1996b	0.27	-53.4^{Q}	5	[IC4-2008: 1.363 1.1]
11265 + 0806	A2575	2013.287	0.418	0.017	49.0*	2.6	USN2002	0.16	−16.9	5	[IC4-2010: 0.42 46.1]
11374 + 4728	KU39	2014.333	1.198	0.007	138.7*	0.3	WSI2006b	0.28	−7.3	5	[IC4-2010: 1.133 129.4]

TABLE 5 (Continued)

WDS	Name	Epoch	ρ (″)	σ_ρ (″)	θ (°)	σ_θ (°)	Orbit	$\Delta\rho_{(O-C)}$ (″)	$\Delta\theta_{(O-C)}$ (°)	Grade	Other measurements, ρ (″) θ (°)
11518 + 5032	HU730	2014.333	0.255	0.047	117.2	1.4	USN2002	0.09	15.1	5	[WDS-2019: 0.2 111]
11541 + 7155	A75	2014.344	0.338	0.017	25.8	1.2	Hei1996a	0.12	−5.7	4	[IC4-1991: 0.143 179.]
12154 + 4008	A1999	2014.324	0.107	0.050	142.8*	8.0	FMR2013d	−0.12	13.7	5	[IC4-2010: 0.22 64.0]
12316 + 3201	COU966	2014.273	0.219	0.027	25.7*	1.1	Mnt1999c	0.09	24.4	5	[IC4-2008: 0.264 28.3]
12316 + 3201	COU966	2014.333	0.278	0.037	27.7*	1.5	Mnt1999c	0.10	26.6	5	[IC4-2008: 0.264 28.3]
13048 + 5555	WOR23	2014.344	1.987	0.010	161.7*	0.3	Izm2019	0.50	−1.4	5	[WDS-2017: 2.0 163.]
13081 + 2657	STT260	2014.341	0.311	0.007	216.9	0.3	Zir2008	−0.02	-37.9^{Q}	3	[IC4-1991: 0.122 218.]
13482 + 2248	COU401	2013.339	0.145	0.050	134.9	8.0	Doc2010h	−0.09	-28.6^{Q}	4	[IC4-2008: 0.492 181.1]
14138 + 3059	COU606	2013.413	0.170	0.007	339.4*	1.6	Doc2018a	0.06	-14.0^{Q}	3	[IC4-2005: 0.162 347]
14142 + 2642	STF1817	2013.429	0.107	0.026	322.2	3.5	Zir2014a	−0.13	−13.4	5	[IC4-2010: 0.17 335.8]
14267 + 1625	A2069	2013.432	0.095	0.015	147.1	8.0	Sca2001g	−0.02	29.6	2	[IC4-2006: 0.206 192.8]
14267 + 1625	A2069	2014.434	0.112	0.018	131.6	8.0	Sca2001g	−0.01	28.0	2	[IC4-2006: 0.206 192.8]
15078 + 3956	COU1271	2014.393	0.418	0.007	194.7*	0.4	Cou1999b	0.04	−26.8	5	[IC4-2010: 0.339 183.1]
16229 + 3803	COU1281	2014.421	0.132	0.007	211.5*	8.0	Doc2012h	0.05	−11.0	3	[IC4-2008: 0.198 195.4]
16229 + 3803	COU1281	2014.429	0.154	0.008	204.6	6.4	Doc2012h	0.08	−17.0	3	[IC4-2008: 0.198 195.4]
16450 + 3842	COU1284	2014.429	0.146	0.050	346.8*	8.0	Cou1999b	0.03	37.6	5	[IC4-2008: 0.177 356]
17141–0824	BAR7	2013.569	1.499	0.007	49.8*	0.3	Cve2008a	−0.12	−5.2	5	[IC4-2013: 1.488 50.0]
17161 + 2316	COU315	2014.543	0.100	0.050	117.2	8.0	Doc2010h	0.01	32.2^{Q}	4	[IC4-2008: 0.125 132.6]
17313 + 1901	COU499	2013.563	0.094	0.050	329.0	8.0	Tok2017c	0.00	−13.4	5	[IC4-2015: 0.093 333.0]
17584 + 0428	KUI84	2013.555	0.156	0.033	371.5*	2.9	Doc2018a	0.05	−28.3	3	[IC4-2015: 0.082 145.1]
18063 + 3824	HU1186	2014.544	0.130	0.020	129.5*	2.3	USN2006b	0.03	−13.4	3	[IC4-2009: 0.30 123.3]
18130 + 3318	COU1006	2014.544	0.490	0.007	332.1*	0.5	Cou1999b	0.25	87.7	5	[IC4-2009: 0.430 320.2]
18178 + 4351	A578Aa,Ab	2014.628	0.330	0.027	243.7*	2.3	Ole2001	0.11	17.4	4	[IC4-2010: 0.31 245.5]
18224 + 4545	A700	2014.639	0.639	0.017	128.4*	0.3	Hei1998	0.51	−28.6	5	[IC4-2013: 0.623 127.9]

TABLE 5 (Continued)

WDS	Name	Epoch	ρ (″)	σ_ρ (″)	θ (°)	σ_θ (°)	Orbit	$\Delta\rho_{(O-C)}$ (″)	$\Delta\theta_{(O-C)}$ (°)	Grade	Other measurements, ρ (″) θ (°)
18363 + 2143	COU206	2013.645	0.096	0.050	149.1*	8.0	Doc2010h	0.04	79.1	4	[IC4-2007: 0.045 289.1]
19069 + 4137	COU2197	2014.582	0.262	0.050	320.1	0.5	Doc2016g	0.09	31.0	5	[IC4-2008: 0.211 168.1]
19180 + 2012	COU321	2013.725	0.107	0.050	140.7	8.0	Doc2003e	−0.04	−19.7	4	[IC4-1998: 0.087 132.8]
19356 + 4002	A1400	2014.628	0.385	0.007	122.4*	0.3	USN2002	0.14	−25.9	5	[IC4-2009: 0.35 122.5]
19458 + 2710	KUI95AB	2013.643	2.204	0.011	59.3*	0.3	Sod1999	−0.17	4.0	5	[IC4-2008: 1.939 55.7]
19458 + 2710	KUI95AB	2014.571	2.217	0.011	59.3*	0.3	Sod1999	−0.21	3.7	5	[IC4-2008: 1.939 55.7]
19474–0148	A2993	2013.629	0.098	0.050	293.9	8.0	Hrt2014b	−0.02	14.1	3	[IC4-2014: 0.109 276.8]
19514 + 4044	COU2530	2014.615	0.107	0.050	119.2	8.0	Tok2019e	−0.01	−13.1	4	[IC4-2008: 0.091 53.4]
20550 + 2805	BU367	2014.833	0.182	0.007	176.3	2.0	Sca2003e	0.03	−21.1	2	[IC4-2012: 0.232 160.4]
21410 + 2920	STT448	2013.818	0.136	0.050	125.0	8.0	Alz2020c	0.01	39.4	3	[IC4-2008: 0.144 140.6]
21410 + 2920	STT448	2014.833	0.100	0.050	31.2	8.0	Alz2020c	−0.03	−43.4	3	[IC4-2008: 0.144 140.6]
21593 + 4606	COU2138	2014.795	0.137	0.050	123.1	8.0	Doc2012c	0.02	14.7	4	[IC4-2008: 0.198 350.8]
22375 + 2356	HU391	2013.818	0.320	0.057	2.5*	1.4	Gur2018	0.09	−11.2	4	[IC4-2009: 0.242 338.2]
23209 + 1643	HEI88	2013.818	0.254	0.027	196.4	2.7	Cve2011a	0.02	11.9^{Q}	3	[WDS-2020: 0.2 211]
23502 + 1940	COU344	2013.818	0.162	0.050	147.3*	4.0	Msn2001a	0.03	17.8^{Q}	5	[IC4-2008: 0.178 324.4]
23502 + 1940	COU344	2014.870	0.175	0.050	139.0	4.0	Msn2001a	0.05	14.1^{Q}	5	[IC4-2008: 0.178 324.4]

*indicates that θ was determined with our quadrant value (or with the long integration).

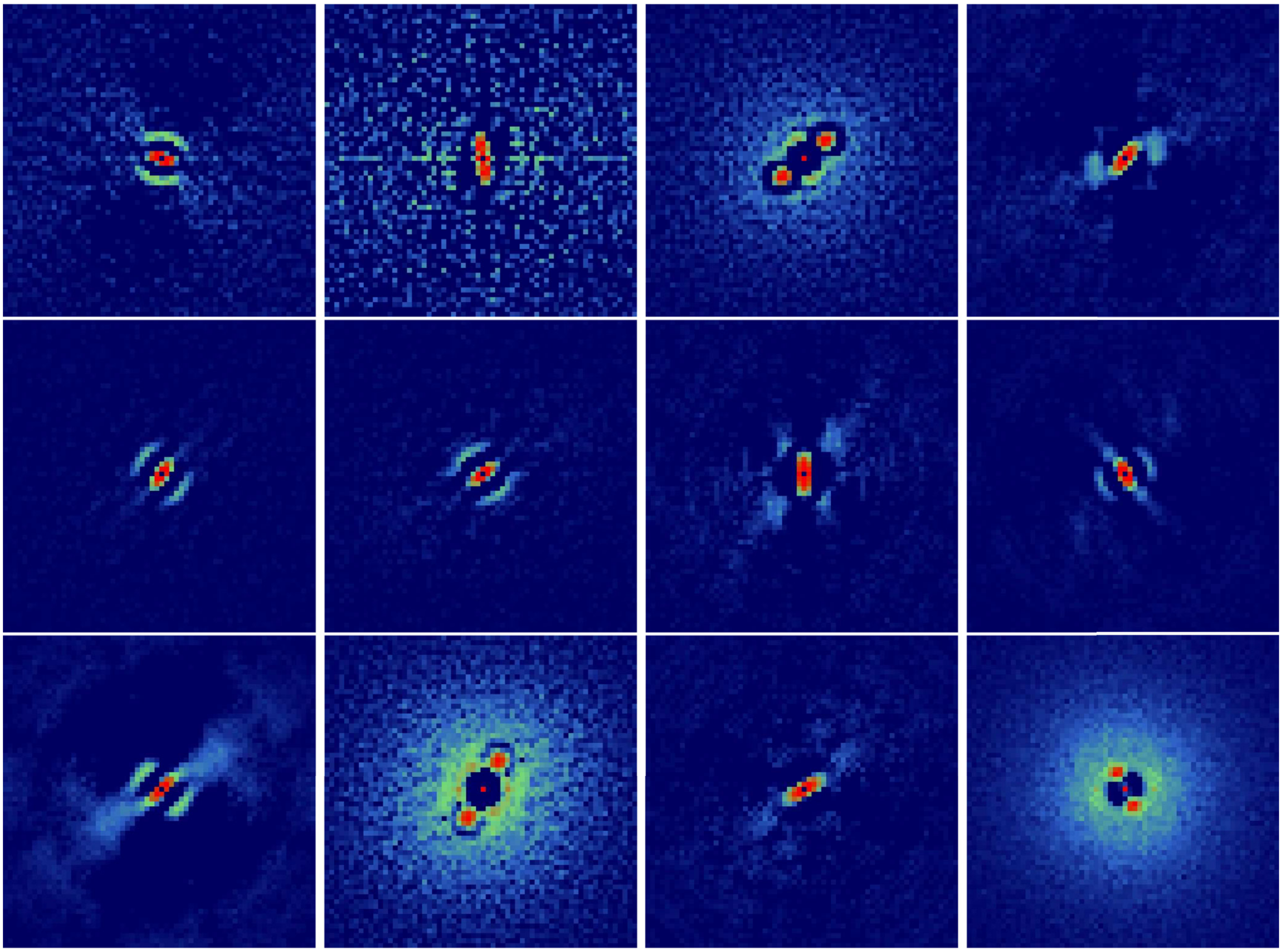

FIGURE 6 Autocorrelations of some double stars with large residuals from Table 5. From left to right and top to bottom: A1061, A1835, A1913, A1999, A2069 (2013, 2014), A2146, BU1058, COU321, COU1006, COU2138, and COU966. North direction is to the bottom and East to the right

For the other objects in that list, the orbits are poorly known, with grades of 4 or 5. Their observations are scarce in the IC4 or the WDS, and only small arcs of orbits have been monitored until now. As shown in Col. 11 of Table 5, our measurements are consistent with those that are reported in the IC4 or the WDS for similar epochs, when available. Clearly, more measurements are needed for obtaining reliable orbits of those objects.

6.3 | Measurements under the diffraction limit

In Table 3, there are 455 measurements with an angular separation smaller than $0''.16$, which is the diffraction limit of our instrumentation (see Section 2.2). Some examples of autocorrelations of those double stars that have been processed with our high-contrast numerical filters are shown in Figure 8. As expected, the autocorrelation peaks are not clearly divided, although the central peak is elongated. Our measurement was made by assuming that the lateral peaks were located on the very edges of that elongated peak.

When an orbit was known, we reported those measurements and the corresponding residuals in Table 6, with the same notation as in Table 3. The mean value of the angular separation from the 58 measurements in this table is $< \rho >= 0''.119 \pm 0''.024$. With a scale of $0''.0738$/pixel (see Section 3), this value corresponds to 1.8 pixels on the autocorrelation frames. The location of the autocorrelation peaks could be estimated with an average error of $0''.016$ (see Section 5). Hence the average error on the position angle corresponds to the angle of $0''.016$ seen at a distance of $0''.133$, which is, therefore: $\arctan(0.016/0.133) \approx 7^{\circ}$.

The residuals from the published orbits of the measurements in Table 6 are plotted in Figure 9. We notice the presence of three outliers, A1061AB, BU1235, and COU206, that have been discussed in the previous section.

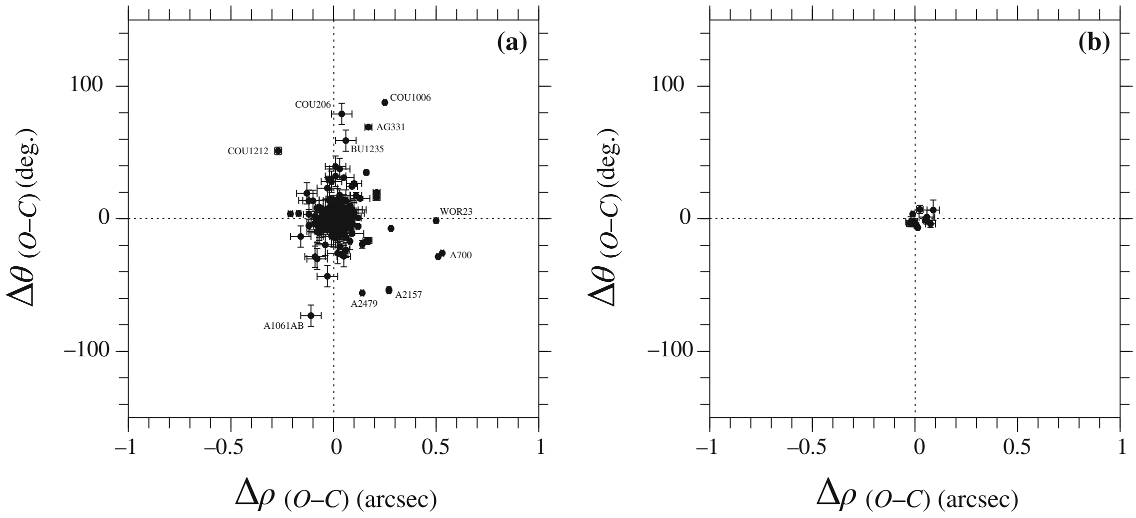

FIGURE 7 Residuals from published orbits of our measurements reported in Table 3: (a) with all orbits, and (b) with the best orbits only (i.e., of Grade 1 in OC6)

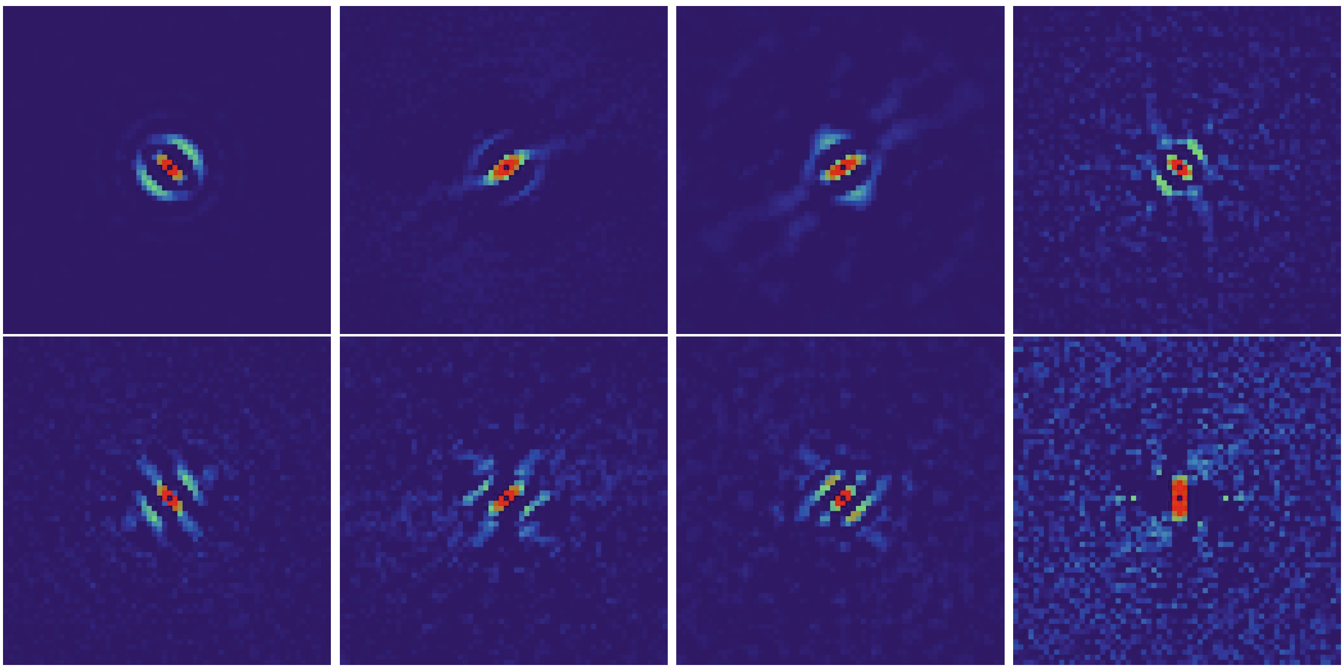

FIGURE 8 Autocorrelations of some double stars with separations smaller than the diffraction limit from Table 6. From left to right and top to bottom: A435, A713, AC8, COU768 (2013), COU768 (2014), HDS1568, HDS2570, and KUI84. North direction is to the bottom and East to the right

The mean values computed with the 58 residuals of Table 6 are $< \Delta\rho_{O-C} >= -0''.008 \pm 0''.052$ and $< \Delta\theta_{O-C} >= 1^\circ.0 \pm 15^\circ.8$ (after rejecting the outliers). Our measurements under the diffraction limit are therefore in good agreement with the ephemerides of published orbits, even though the uncertainties larger in this case (as shown above, the expected average errors are $0''.02$ for ρ and 7° for θ). Those measurements have been made possible by good observations obtained under good seeing conditions and by the use of efficient high-contrast filters (see Paper III).

7 | CONCLUSION

In 2013–2014, we obtained 4,952 new position measurements of 4,864 visual double stars or multiple systems with

TABLE 6 Measurements and residuals of the closest binaries observed in 2013–2014, with ρ < 0″.16 (i.e., smaller than the diffraction limit), for the objects having a known orbit

WDS	Name	Epoch	ρ (″)	θ (°)	Orbit	$\Delta\rho_{(O-C)}$ (″)	$\Delta\theta_{(O-C)}$ (°)
00055 + 3406	HU1201	2014.828	0.147	310.6	Zir2003	−0.01	3.8
00274 + 3054	HDS62	2013.946	0.080	314.0	Ren2013	0.05	3.3
01570 + 3101	A819	2013.963	0.140	0.6*	Hrt2009	−0.10	12.6
03423 + 3141	COU691	2014.976	0.147	269.5	Doc2010d	0.06	−6.0
04245 + 2244	BU1235	2013.016	0.125	327.2	Zir2010	0.06	59.0
04445 + 3953	COU1524	2014.119	0.098	62.7	Doc2019f	−0.03	23.1^{Q}
05048 + 1319	HEI104	2014.149	0.090	195.5	Tok2019c	−0.02	8.6
06105 + 2300	BU1058	2014.182	0.082	206.5*	FMR2014b	−0.07	-10.6^{Q}
06503 + 2409	COU768	2013.172	0.117	60.70	Doc2003e	−0.03	0.6^{Q}
06503 + 2409	COU768	2014.201	0.111	44.1	Doc2003e	−0.01	-7.1^{Q}
06594 + 2514	A1061AB	2014.146	0.083	73.2	USN2002	−0.11	−73.1
08539 + 1958	COU773	2014.198	0.079	74.2	Cou1999b	−0.10	13.6
08585 + 3548	COU1897	2013.196	0.142	305.7	Doc2013b	0.06	13.8
09179 + 2834	STF3121	2014.182	0.151	176.8*	Sod1999	−0.04	6.5^{Q}
09477 + 2036	COU284	2013.287	0.139	149.0	Doc2019c	0.02	-26.0^{Q}
10121 + 2118	A2146	2013.287	0.113	179.9	Hei2001	−0.08	−30.3
10264 + 2545	HDS1500	2014.308	0.105	286.5	Tok2019c	−0.03	−2.5
10596 + 1800	HDS1568	2013.287	0.100	316.7	Tok2019d	0.03	−9.0
11322 + 3615	HU1134AB	2014.240	0.117	115.1	Hrt2000b	0.01	-6.2^{Q}
11518 + 5032	HU730	2014.308	0.085	92.5	USN2002	−0.08	−9.7
12154 + 4008	A1999	2014.324	0.107	142.8*	FMR2013d	−0.12	13.7
12409 + 2708	COU596	2014.273	0.130	197.1*	Doc2013a	−0.05	−3.7
12508 + 0806	HDS1803	2013.295	0.132	49.8*	Tok2018e	−0.07	−8.4
13482 + 2248	COU401	2013.339	0.145	134.9	Doc2010h	−0.09	-28.6^{Q}
14124 + 2843	STT277	2013.429	0.151	36.6*	Ole2002d	0.10	4.3^{Q}
14142 + 2642	STF1817	2013.429	0.107	322.2	Zir2014a	−0.13	−13.4
14267 + 1625	A2069	2013.432	0.095	147.1	Sca2001g	−0.02	29.6
14267 + 1625	A2069	2014.434	0.112	131.6	Sca2001g	−0.01	28.0
15106 + 2021	HU144	2014.434	0.148	314.5	Tok2020g	0.06	5.8
15379 + 5005	HDS2203	2014.412	0.107	296.1	Cve2013b	0.00	8.1^{Q}
15420 + 4203	COU1445	2014.429	0.136	200.9	Doc2013e	0.02	−7.7
16229 + 3803	COU1281	2014.421	0.132	211.5*	Doc2012h	0.05	−11.0
16229 + 3803	COU1281	2014.429	0.154	204.6	Doc2012h	0.08	−17.0
16450 + 3842	COU1284	2014.429	0.146	346.9*	Cou1999b	0.03	37.6
17161 + 2316	COU315	2014.543	0.100	117.2	Doc2010h	0.01	32.2^{Q}
17313 + 1901	COU499	2013.563	0.094	329.0	Tok2017c	0.00	−13.4
17529 + 2941	AC8	2014.546	0.111	304.4	Zir2014a	0.04	−7.7
17533 + 2459	A235	2013.645	0.102	49.0*	Hrt2014b	−0.08	−3.5

TABLE 6 (Continued)

WDS	Name	Epoch	ρ ($''$)	θ (°)	Orbit	$\Delta\rho_{(O-C)}$ ($''$)	$\Delta\theta_{(O-C)}$ (°)
17563 + 0259	A2189	2013.588	0.122	97.9	Doc2018l	0.01	-0.9^Q
17584 + 0428	KUI84	2013.555	0.156	371.5*	Doc2018a	0.05	−28.3
18063 + 3824	HU1186	2014.544	0.130	129.5*	USN2006b	0.03	−13.4
18121 + 4644	COU2118	2014.639	0.129	274.0*	Cou1999b	−0.01	-0.2^Q
18126 + 1224	HDS2570	2013.640	0.086	320.0	Tok2020g	−0.01	3.7
18181–0120	HDS2587Aa,Ab	2013.643	0.086	318.7	Tok2018e	−0.01	2.4
18363 + 2143	COU206	2013.645	0.096	149.1*	Doc2010h	0.04	79.1
19180 + 2012	COU321	2013.725	0.107	140.7	Doc2003e	−0.04	−19.7
19313 + 4729	A713	2014.637	0.126	304.0*	Zas2012c	−0.06	−6.0
19474–0148	A2993	2013.629	0.098	293.9	Hrt2014b	−0.02	14.1
19514 + 4044	COU2530	2014.615	0.107	119.2	Tok2019e	−0.01	−13.1
20311 + 1548	A1675	2014.833	0.154	311.0	Hrt2001b	−0.01	4.8
21125 + 2821	HO152	2014.659	0.111	145.5*	Doc2016g	−0.05	−0.7
21410 + 2920	STT448	2013.818	0.136	125.0	Alz2020c	0.01	39.4
21410 + 2920	STT448	2014.833	0.100	31.2	Alz2020c	−0.03	−43.4
21510 + 2911	A889	2013.818	0.151	328.8	Baz1984b	0.04	9.7^Q
21593 + 4606	COU2138	2014.795	0.137	123.1	Doc2012c	0.02	14.7
23199 + 2844	COU439	2014.774	0.130	3.6	Doc2017e	−0.01	2.0
23424 + 3903	A1494	2013.946	0.136	173.0	Gur2020	0.03	9.4^Q
23424 + 3903	A1494	2013.946	0.148	172.0	Gur2020	0.04	8.4^Q

Note: In column 5, the * indicates that the position angle θ could be determined without the 180° ambiguity. In column 8, the superscript Q indicates that our θ measurement quadrant was not compatible with the quadrant used for computing the orbit.

the 76-cm refractor in Nice. The average accuracy is estimated at $0''.015$ for the angular separations and $1°.0$ for the position angles. We have been able to routinely monitor faint systems $m_V = 9$–11 even for objects with a large magnitude difference (up to $\Delta m_V = 4.5$). The color-magnitude diagram of our observations shows that we have thus been able to measure red dwarf stars that had been poorly monitored until now. We have thus been able to measure 49 systems containing red dwarf stars that have been poorly monitored since their discovery, from which we have estimated the stellar masses thanks to Gaia measurements.

By using the DVA method, we have measured the difference in magnitude of the two components for 326 objects with an estimated error of 0.2 mag. Thanks to good seeing images and with the use of high-contrast numerical filters, we have also been able to obtain 455 measurements with an angular separation smaller than the diffraction limit of our instrumentation and consistent with those obtained with larger telescopes. We also report 378 measurements of the 296 new double stars that we found in the files obtained during the observations.

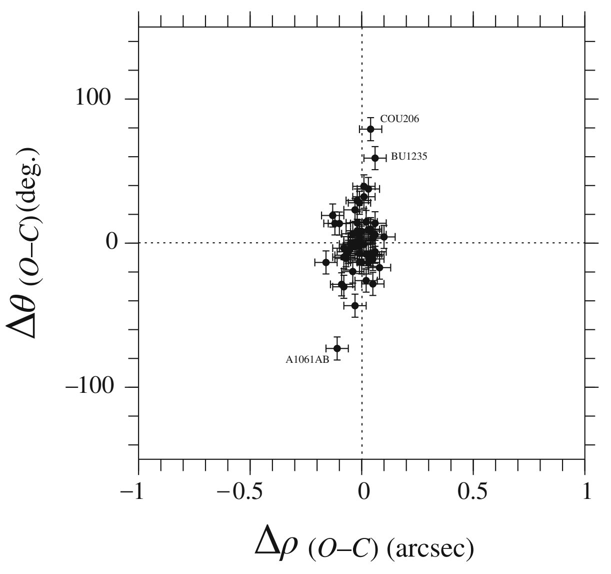

FIGURE 9 Residuals from published orbits of our measurements with angular separations smaller than the diffraction limit (from Table 6, with all orbits)

This work is thus a good contribution to the continuous monitoring of long-period visual binary systems, which is important for refining systemic stellar masses. It validates the technical and data processing investments that we have made in the preceding years. This work is fully integrated into the observation efforts of Commission G1, "Binary and Multiple Star Systems" of the International Astronomical Union. Our measurements will be added to the worldwide database of this Commission G1, which is currently maintained by the U.S. Naval Observatory.

ACKNOWLEDGMENTS

The authors are indebted to the directors of Observatoire de la Côte d'Azur for allowing us to use the 76-cm refractor and to the staff of this observatory for their technical support. The authors thank G. Morlet for writing a program dedicated to the 76-cm refractor that was used for pointing stars with the telescope. The authors are grateful to F. Losse for adapting the REDUC software to our needs and to C. Buil for providing his IRIS software to the amateur community (Buil 2022). This work has made use of the "Fourth Catalogue of Interferometric Measurements of Binary Stars" (http://www.astro.gsu.edu/wds/int4.html), the "Sixth Catalogue of Orbits of Visual Binary Stars" (http://www.astro.gsu.edu/wds/orb6.html), the Washington Double Star Catalog maintained at the U.S. Naval Observatory (http://www.astro.gsu.edu/wds), the SIDONIe (Site Informatique des étoiles DOubles de Nice; http://sidonie.obs-nice.fr), and the SIMBAD database (http://simbad.u-strasbg.fr/simbad) operated by the Centre de Données Astronomiques de Strasbourg (France).

REFERENCES

ANDOR. 2022, ANDOR technology, http://www.andor-tech.com

Angelov, T. 1993, *Bull. Astron. Belgrade*, *148*, 1.

Bagnuolo, W. G., Mason, B. D., Barry, D. J., Hartkopf, W. I., & McAlister, H. A. 1992, *AJ*, *103*, 1399.

Buil, C. 2022, IRIS software, http://www.astrosurf.com/buil/us/iris/iris.htm

ESA. 2022, Gaia Archive DR2, 2nd release, http://gea.esac.esa.int/archive/

Gili, R. 2016, *IAU Commission G1 - Double Stars Inf. Circ.*, *190*, 4.

Gili, R., & Prieur, J.-L. 2012, *Astron. Nachr.*, *333*, 727 (Paper I).

Gili, R., Prieur, J.-L., Rivet, J.-P., Vakili, F., Koechlin, L., & Bonneau, D. 2014, *Observatory*, *134*, 267.

Gili, R., Prieur, J.-L., Rivet, J.-P., et al. 2020, *Astron. Nachr.*, *341*, 441 (Paper II).

Gili, R., Prieur, J.-L., Rivet, J.-P., et al. 2021, *Astron. Nachr.*, *342*, 865 (Paper III).

Hartkopf, W. I., Mason, B. D., & Worley, C. E. 2001, *Astron. J.*, *122*, 3472.

Hartkopf, W. I., Mason, B. D., & McAlister, H. A. 2020, Fourth Catalogue of Interferometric Measurements of Binary Stars http://www.astro.gsu.edu/wds/int4.html (IC4).

Labeyrie, A. 1970, *A&A*, *6*, 85.

Losse, F. 2022, REDUC, data processing software, http://www.astrosurf.com/hfosaf/

Malkov, O. Y. 2012, *A&A*, *546*, 69.

Mason, B. D., Wycoff, G. L., & Hartkopf, W. I. 2022, Washington Double Star Catalogue, http://www.astro.gsu.edu/wds/ (WDS).

Matson, R. A., Williams, S. J., Hartkopf, W. I., & Mason, B. D. 2022. Sixth Catalogue of Orbits of Visual Binary Stars, http://www.astro.gsu.edu/wds/orb6.html (OC6).

Michelson, A. A. 1890, *Philosophical Magazine*, 5th series, Vol. *30*, Philosophical Magazine and Journal of Science (London), 1.

Parent, I., Vaughn, S., Conover, E., et al. 2017, *JDSO*, *13*, 384.

Pribulla, T. 2006, *AJ*, *131*, 296.

Scardia, M., Prieur, J.-L., Pansecchi, L., & Argyle, R. W. 2008, *Astron. Nachr.*, *329*(4), 379.

Scardia, M., Rivet, J.-P., Prieur, J.-L., et al. 2019, *Astron. Nachr.*, *340*, 771.

Straizys, V., & Kuriliene, G. 1981, *Astrophys. Space Sci.*, *80*, 353.

Worden, S. P., Murray, K. S., Schmidt, G. D., & Angel, J. R. P. 1977, *Icarus*, *32*, 450.

AUTHOR BIOGRAPHY

René Gili (1951–2018) is a French amateur astronomer who made thousands of astronomical observations of double stars with the 0.50m and the 0.76m refractors of Nice Observatory, first with a micrometer and later with electronic imaging sensors.

SUPPORTING INFORMATION

Additional supporting information can be found online in the Supporting Information section at the end of this article.

How to cite this article: Gili, R., Prieur, J.-L., Rivet, J.-P., et al. 2022, *Astron. Nachr.*, *343*, e20224008. https://doi.org/10.1002/asna.20224008